Supplementary Figures

Spatially Stereotyped Microgliosis Tracks Synaptic Pathology in the Demyelinated Superior Colliculus

Jackson David McGrath[1], John Shultz[1,*], Maia Jin Classe[1,*], D. Ford Hannum[1], Sebastian Werneburg[1,2,3,#]

AFFILIATIONS

[1] Department of Ophthalmology and Visual Sciences, Michigan Medicine, University of Michigan, 1000 Wall Street, Ann Arbor, MI 48105, USA
[2] Department of Molecular & Integrative Physiology, Michigan Medicine, University of Michigan, 1137 E. Catherine Street, Ann Arbor, MI 48109, USA
[3] Neuroscience Institute, Michigan Medicine, University of Michigan, Ann Arbor, MI 48109, USA

*** Equally Contributing Authors**

 # Corresponding Author

Corresponding Author Contact Details:

Sebastian Werneburg, Ph.D.

email: wernebur@umich.edu

phone: 508-826-3045

fax: 734-232-8021

Neurological Diagnosis	Sex	Age (years)	Optic Neuritis History	Postmortem Delay (hours)
None	Male	39	No	Unknown
None	Male	47	No	23
None	Male	59	No	12
None	Male	65	No	24
None	Male	65	No	26
None	Female	73	No	14
Multiple sclerosis	Male	49	Unknown	22
Multiple sclerosis	Female	69	Unknown	22
Multiple sclerosis	Female	69	Yes	30

Supplementary Table 1: Human Postmortem Tissue Source Information.

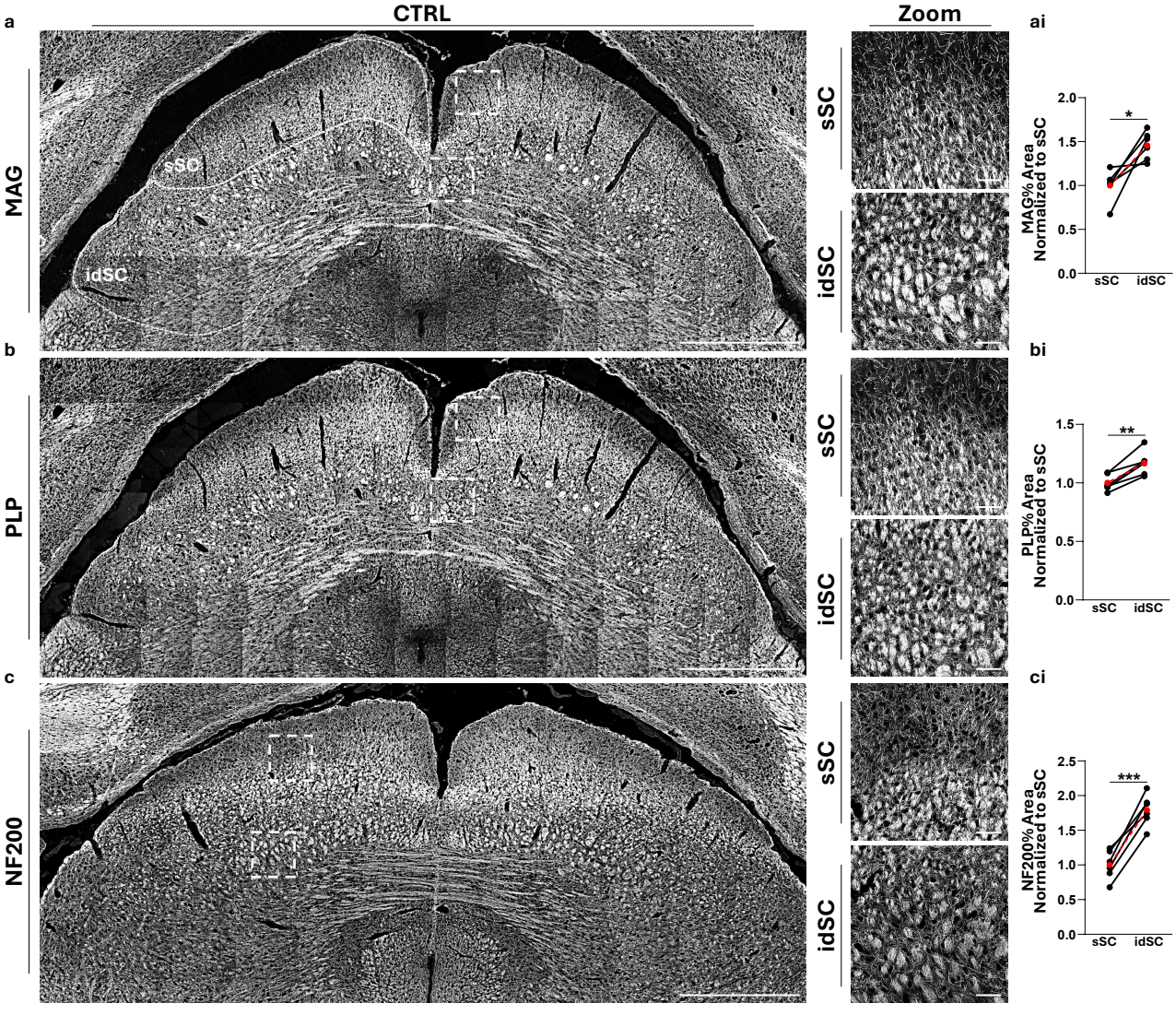

Supplementary Figure 1: Baseline Myelin and Axonal Density Differ Between Superficial and Intermediate/Deep SC Layers. (**a-c**) Representative tiled images of the entire SC from CTRL mice showing (**a**) MAG, (**b**) PLP, and (**c**) NF200. Detailed view of all markers (white boxes) in the sSC and idSC (dashed outlines) is shown in higher magnification images (Zoom). Quantifications of (**ai**) MAG$^+$-myelin density, (**bi**) PLP$^+$-myelin density, and (**ci**) NF200$^+$-axon density show higher myelin and axonal densities in the idSC compared to the sSC at baseline (normalized to sSC). Scale bars, 500 µm (tiled) and 40 µm (zoom). n = 6 mice. Data represent mean ± SEM; significant differences with (∗) $p < 0.05$, (∗∗) $p < 0.01$, (∗∗∗) $p < 0.001$. t-test, paired.

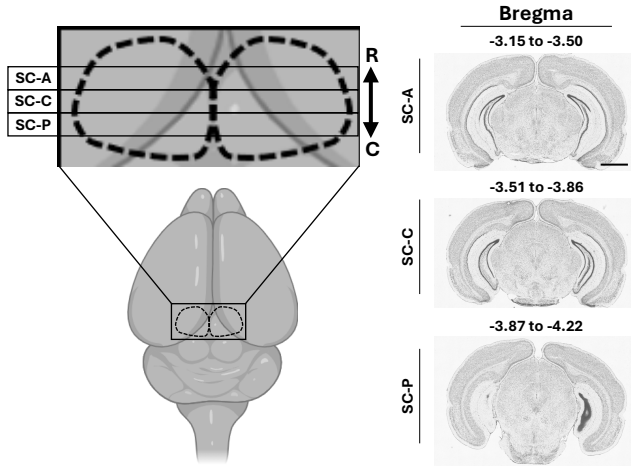

Supplementary Figure 2: Rostro–caudal Sampling Strategy for Anterior, Central, and Posterior SC Planes. Mouse brain schematic defining anterior (SC-A, Bregma -3.15 to -3.5), central (SC-C, Bregma -3.51 to -3.86), and posterior (SC-P, Bregma -3.87 to -4.22) coronal planes of the SC along the rostro–caudal brain axis. Representative coronal sections from Paxinos Mouse Brain Atlas [51] corresponding to the respective SC regions. Scale bar, 500 μm. The brain schematic was created with BioRender.com

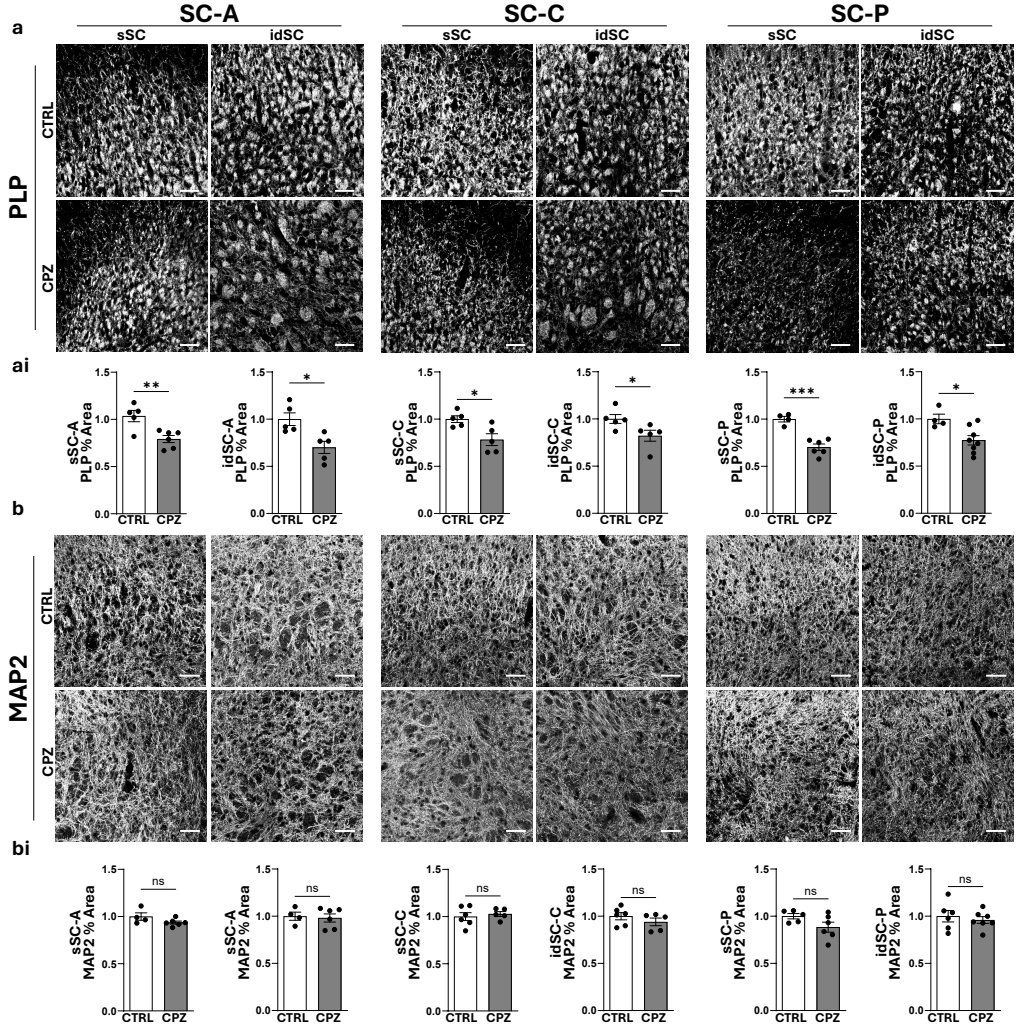

Supplementary Figure 3: PLP Loss Confirms Widespread SC Demyelination After CPZ Without Detectable MAP2 Alterations. Analysis of adjacent SC-A, SC-C, and SC-P sections from the same mice as shown in Figs. 2-5. (**a-b**) Representative sSC and idSC images from CTRL or CPZ-treated mice along the rostro–caudal axis showing (**a**) PLP and (**b**) the microtubule marker MAP2. Quantifications of (**ai**) PLP^{+}-myelin density (normalized to CTRL) show widespread demyelination in the sSC and idSC across all rostro–caudal planes of CPZ-treated animals compared to CTRL. Quantifications of (**bi**) MAP2^{+}-microtubule density (normalized to CTRL) show no detectable change in microtubule densities across the SC following CPZ treatment compared to CTRL. Scale bars, 40 µm. n = 4-8 mice. Data represent mean ± SEM; ns, non-significant results, significant differences with (∗) $p < 0.05$, (∗∗) $p < 0.01$, (∗∗∗) $p < 0.001$. t-test, unpaired.

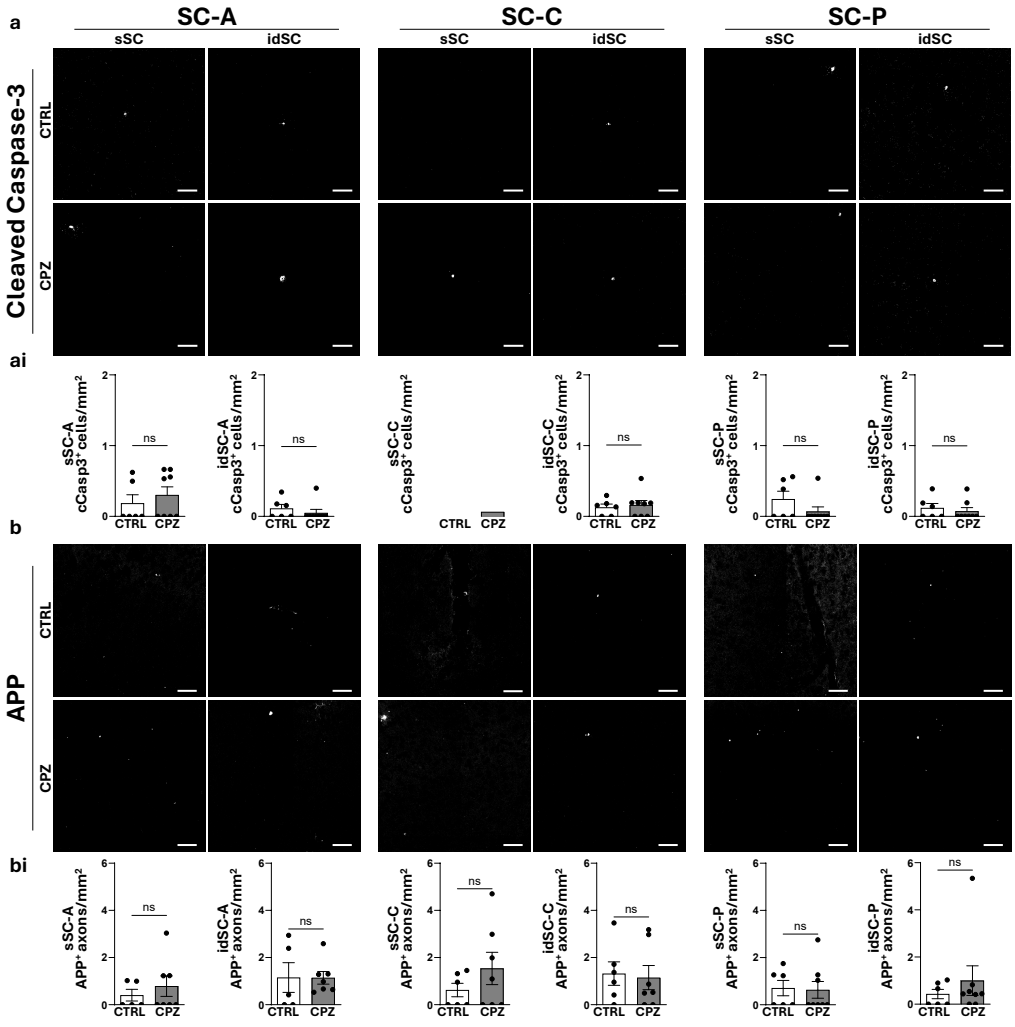

Supplementary Figure 4: CPZ Treatment Does Not Induce Detectable Apoptosis or Axonal Pathology in the SC. Analysis of adjacent SC-A, SC-C, and SC-P sections from the same mice as shown in Figs. 2-5. (**a-b**) Representative sSC and idSC images from CTRL or CPZ-treated mice along the rostro–caudal axis showing (**a**) the apoptotic marker cleaved caspase-3 (cCasp3) and (**b**) the axonal degeneration marker amyloid precursor protein (APP). Quantifications of (**ai**) cCasp3^{+}-apoptotic cell count and (**bi**) APP^{+}-degenerating axon count show no detectable change in apoptosis or axon degeneration across the SC following CPZ treatment compared to CTRL. Scale bars, 40 µm. n = 5-8 mice. Data represent mean ± SEM; ns, non-significant results. t-test, unpaired.

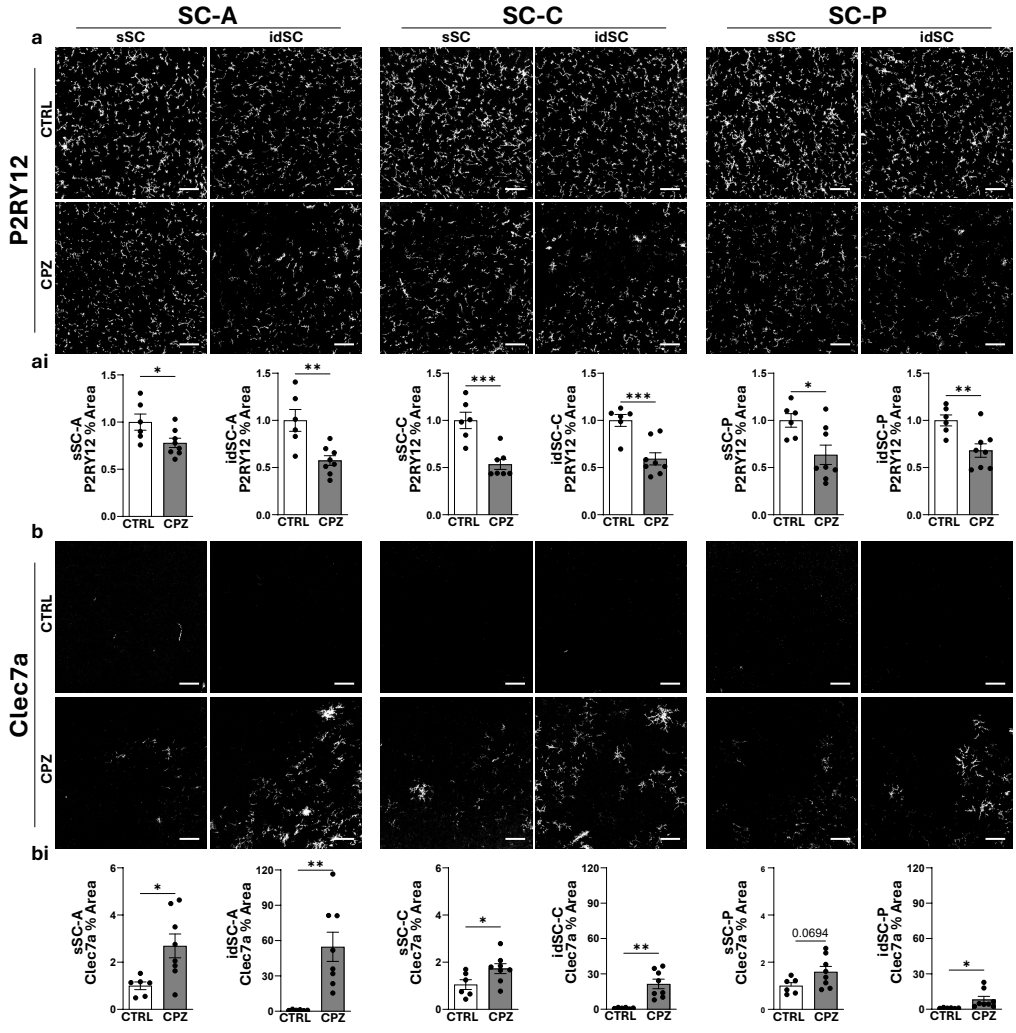

Supplementary Figure 5: CPZ Induces Widespread Microglial Reactivity Across SC Layers and the Rostro–caudal Axis. Analysis of adjacent SC-A, SC-C, and SC-P sections from the same mice as shown in Figs. 2-5. (**a-b**) Representative sSC and idSC images from CTRL or CPZ-treated mice along the rostro–caudal axis showing (**a**) homeostatic microglia marker P2RY12 and (**b**) reactive microglia marker Clec7a. Quantifications show (**ai**) a reduction in P2RY12^{+}-microglia density and (**bi**) an increase in Clec7a^{+}-microglia density in the sSC and idSC across all rostro–caudal planes (normalized to CTRL). Scale bars, 50 µm. n = 6-8 mice. Data represent mean ± SEM; significant differences with (∗) $p < 0.05$, (∗∗) $p < 0.01$, (∗∗∗) $p < 0.001$. t-test, unpaired.

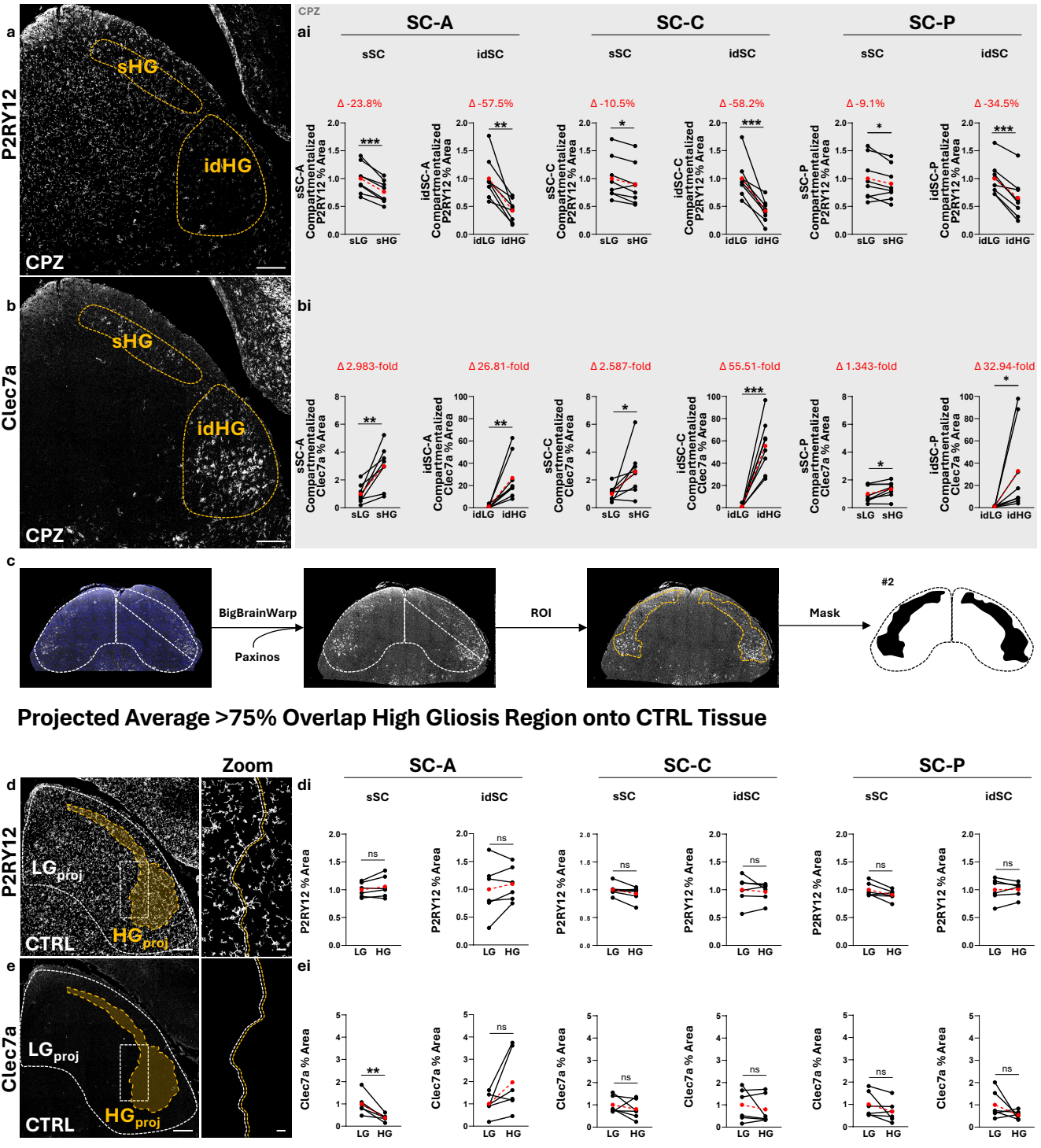

Supplementary Figure 6: HG Regions Span sSC and idSC Layers and Are Not Explained by Baseline Differences in Microglial State. Analysis of adjacent SC-A, SC-C, and SC-P sections from the same mice as shown in Figs. 2-5. (**a,b**) Representative tiled SC-C images of the entire SC from CPZ-treated mice with HG regions (dashed orange outline) separated by the sSC (sHG) and idSC (idHG) showing (**a**) P2RY12 and (**b**) Clec7a. Comparative assessment of (**ai**) P2RY12^{+}-

Suppl. Fig. 6 continued:

microglia density and (**bi**) Clec7a^{+}-microglia density in sLG, sHG, idLG, and idHG regions revealed significant alterations across SC layers and the rostro–caudal axis (normalized to the LG region). Delta values represent the average (**ai**) % reduction in P2RY12 and (**bi**) fold increase in Clec7a compared to adjacent LG regions. (**c**) Schematic of the BigBrainWarp workflow used to generate atlas-aligned HG ROI masks (example shown for CPZ animal #2, see Methods). (**d,e**) Representative tiled SC-C image of the entire SC (dashed white outline) from CTRL-treated mice with the projected >75% HG region affected in the majority of CPZ-treated mice (HG_{proj}, dashed orange outline) showing (**d**) P2RY12 and (**e**) Clec7a. SC area unoccupied by HG_{proj} was defined as the projected LG region (LG_{proj}). Higher magnification images (Zoom) outline the border between the HG_{proj} and the LG_{proj} regions in control tissue (dashed white box). Comparative assessment of (**di**) P2RY12^{+}-microglia density and (**ei**) Clec7a^{+}-microglia density revealed no differences between the projected HG and LG regions at baseline in healthy CTRL animals (normalized to LG_{proj} region). Scale bars, 200 µm (tiled) and 20 µm (zoom). n = 6-8 mice. Data represent mean ± SEM; red data points visualize average values for each designated group; ns, non-significant results, significant differences with (∗) $p < 0.05$, (∗∗) $p < 0.01$, (∗∗∗) $p < 0.001$. t-test, paired.

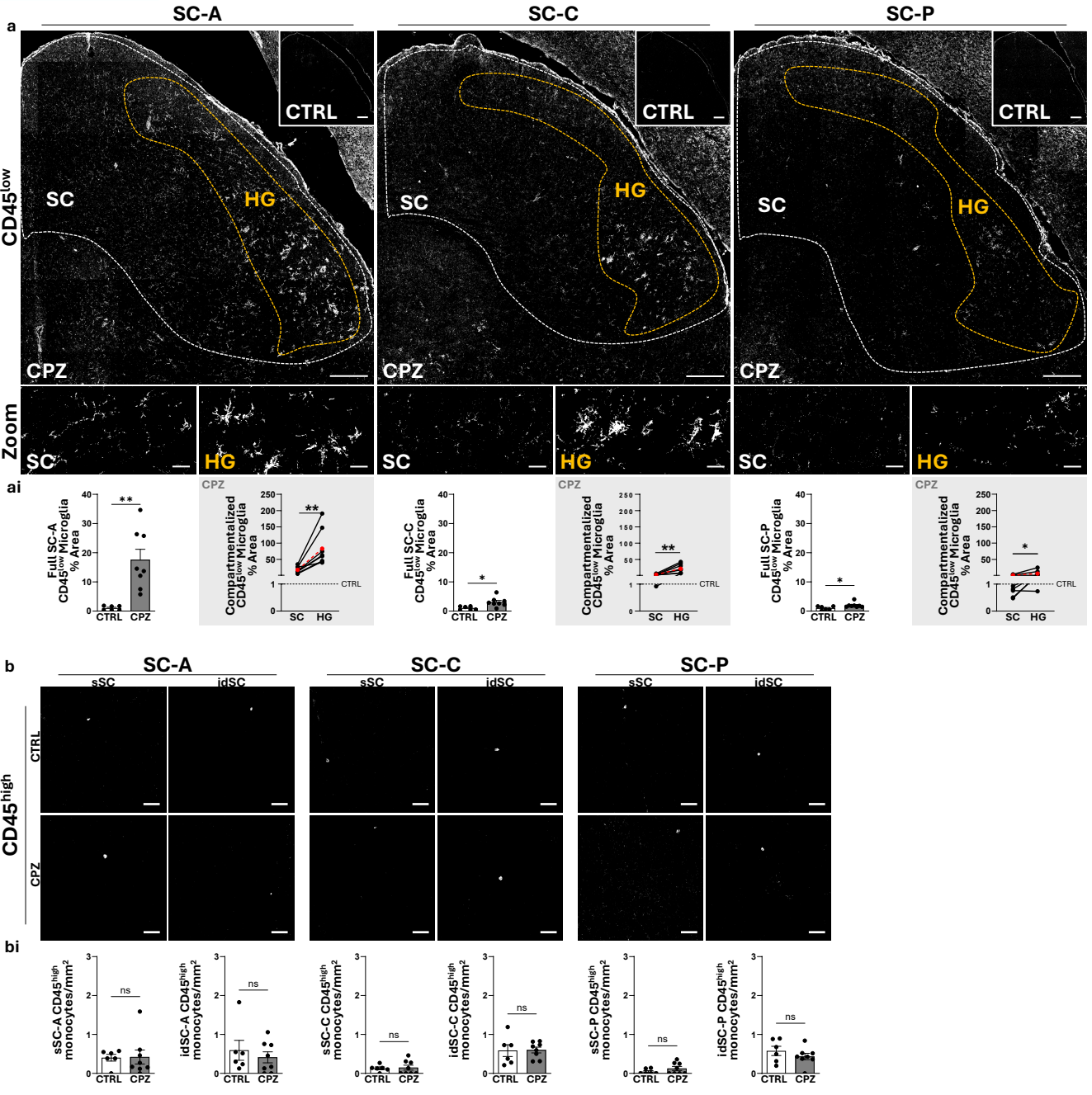

Supplementary Figure 7: CD45 Staining Supports Local Microglial Reactivity Without Detectable Peripheral Immune Cell Accumulation in the SC. Analysis of adjacent SC-A, SC-C, and SC-P sections from the same mice as shown in Figs. 2-5. (**a**) Representative tiled images of the entire SC along the rostro–caudal axis from CTRL or CPZ-treated mice showing the leukocyte marker CD45. The SC is denoted by a white dashed line, and quantifications across the full SC (SC) identified (**ai**) an increase in CD45^{low}-microglia/macrophage density following CPZ treatment across all rostro–caudal planes (graphs on white background, normalized to CTRL). Closer inspection of full SC-tiles confirmed the discrete high-microgliosis compartment (HG, orange outline) spanning

Suppl. Fig. 7 continued:

parts of both the sSC and idSC in CPZ-animals. Within CPZ tissue, the HG compartments showed an especially pronounced increase in $CD45^{low}$ microglia compared to the full SC (graphs on gray background, normalized to CTRL). (**b**) Representative images along the rostro–caudal axis in the sSC and the idSC from CTRL or CPZ-treated mice showing $CD45^{high}$ round monocytes. Quantifications of (**bi**) $CD45^{high}$-monocyte counts show no detectable change in monocyte infiltration across the SC following CPZ treatment compared to CTRL. Scale bars, 200 µm (**a**, tiled), 20 µm (**a**, zoom), 40 µm (**b**). n = 6-8 mice. Data represent mean ± SEM; red data points visualize average values for each designated group, ns, non-significant results, significant differences with (∗) $p < 0.05$, (∗∗) $p < 0.01$. t-test, unpaired (graphs on white background), paired (graphs on gray background).

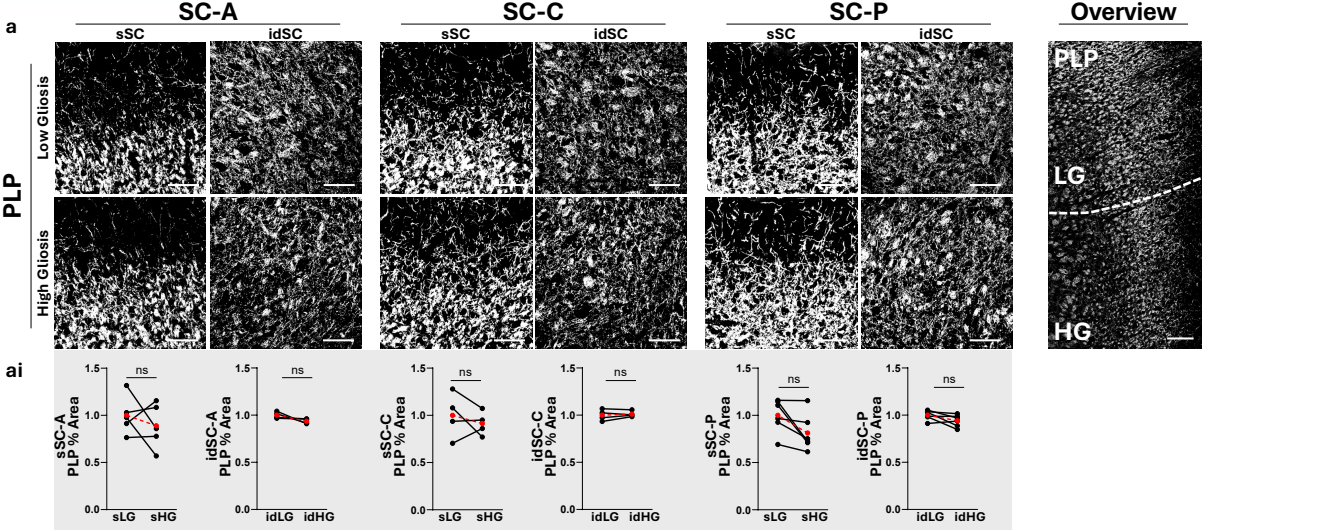

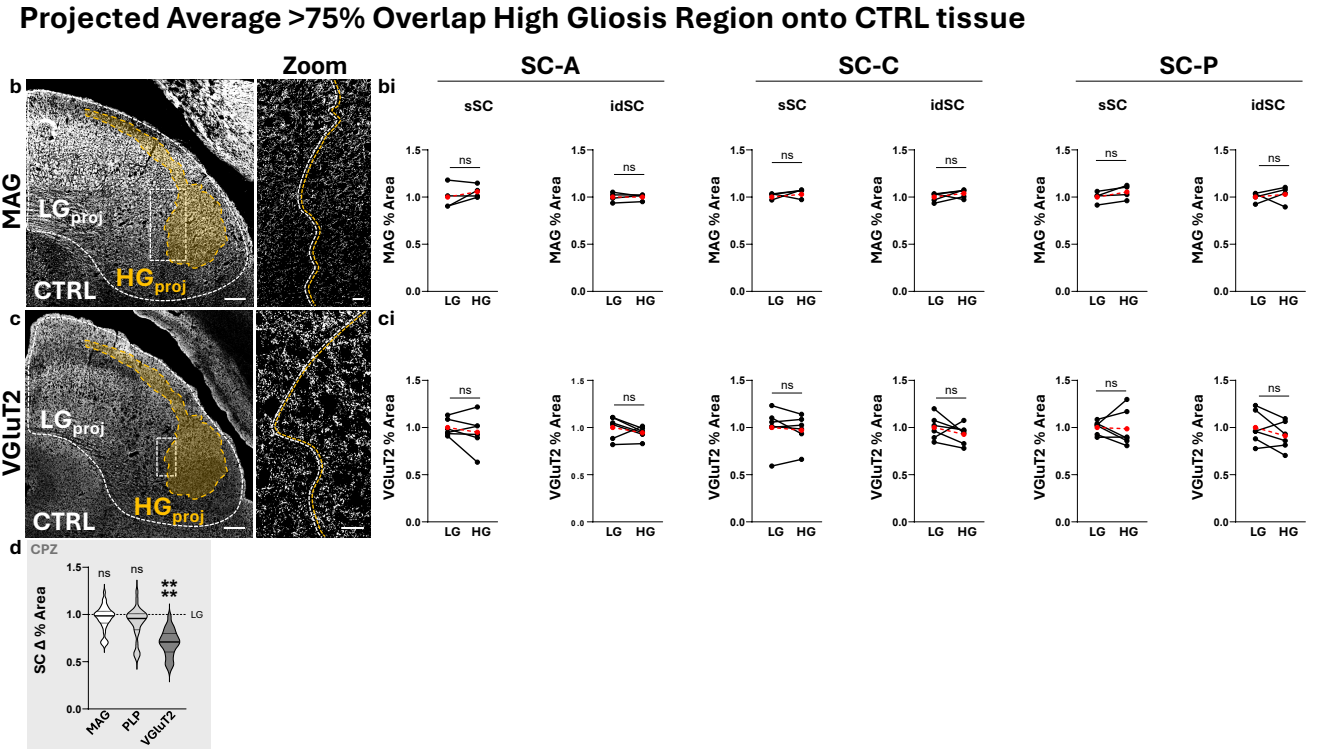

Supplementary Figure 8: HG Regions With Heightened Synaptic Loss Show No Differences in Local Myelin Loss or Baseline Myelin and Synaptic Architecture. Analysis of adjacent SC-A, SC-C, and SC-P sections from the same mice as shown in Figs. 2-5. (**a**) Representative images along the rostro–caudal axis from CPZ-treated mice in low-gliosis (LG) and high-gliosis (HG) regions of the sSC and idSC showing PLP. An SC overview image illustrating no differences in PLP^{+}-myelin densities in LG compared to HG regions following CPZ. (**ai**) Comparative assessment of PLP^{+}-myelin density in superficial (s) or intermediate/deep (id) regions with LG or HG revealed no differences (normalized to the LG region). (**b,c**) Representative tiled SC-C images of the entire SC (dashed white outline) from CTRL-treated mice with the projected >75% HG region affected in the majority of CPZ-treated mice (HG_{proj}, dashed orange outline) showing (**b**) MAG and (**c**) VGluT2. SC area unoccupied by HG_{proj} was

Suppl. Fig. 8 continued:

defined as the projected LG region (LGproj). Higher magnification images (Zoom) outline the border between the HG_{proj} and the LG_{proj} regions in control tissue (dashed white box). Comparative assessment of (**bi**) MAG^{+}-myelin density and (**ci**) $VGluT2^{+}$-synaptic density revealed no differences between the HG_{proj} and LG_{proj} regions (normalized to the LG_{proj} region). (**d**) Within CPZ-treated mice, HG regions show comparable myelin loss (MAG, PLP) but more synaptic damage (VGluT2) compared to LG regions (normalized to LG). Scale bars, 50 µm (**a**) and 100 µm (overview), 200 µm (**tiled**), 20 µm (**zoom**). n = 4-6 mice. Data represent mean ± SEM; red data points visualize average values for each designated group, ns, non-significant results, significant differences with (∗∗∗∗) $p < 0.0001$. t-test, paired.